ChemComm

Accepted Manuscript

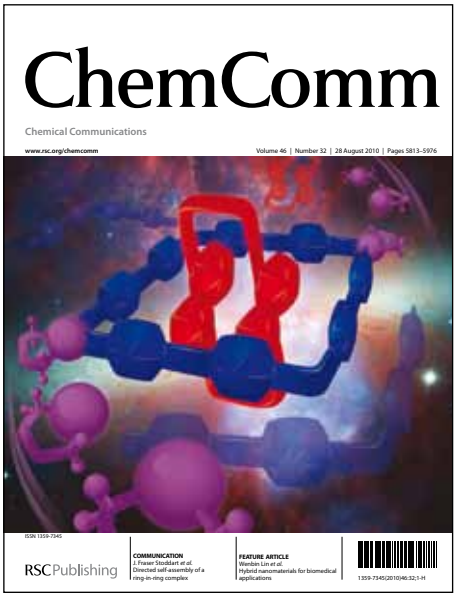

This is an *Accepted Manuscript*, which has been through the RSC Publishing peer review process and has been accepted for publication.

Accepted Manuscripts are published online shortly after acceptance, which is prior to technical editing, formatting and proof reading. This free service from RSC Publishing allows authors to make their results available to the community, in citable form, before publication of the edited article. This *Accepted Manuscript* will be replaced by the edited and formatted *Advance Article* as soon as this is available.

To cite this manuscript please use its permanent Digital Object Identifier (DOI®), which is identical for all formats of publication.

More information about *Accepted Manuscripts* can be found in the **Information for Authors**.

Please note that technical editing may introduce minor changes to the text and/or graphics contained in the manuscript submitted by the author(s) which may alter content, and that the standard **Terms & Conditions** and the **ethical guidelines** that apply to the journal are still applicable. In no event shall the RSC be held responsible for any errors or omissions in these *Accepted Manuscript* manuscripts or any consequences arising from the use of any information contained in them.

Journal Name ChemComm Dynamic Article Links ►

Cite this: DOI: 10.1039/c0xx00000x

www.rsc.org/xxxxxx

ARTICLE TYPE

The first decade of Organic Spintronics research

Dali Sun,[a] Eitan Ehrenfreund,[b] and Z. Valy Vardeny*[a]

Received (in XXX, XXX) Xth XXXXXXXXX 20XX, Accepted Xth XXXXXXXXX 20XX
DOI: 10.1039/b000000x

The first decade of organic spintronics research has benefitted from the analogy and previous experience of the inorganic spintronics field, coupled with the unlimited versatility of organic materials synthesis. At the same time, the field of organic spintronics has developed to be an attractive and promising field of its own, with rich physics and promising unique potential applications. We review here a set of significant milestones achieved in organic spintronics devices such as organic spin valves, bipolar spin-valves, and hybrid organic/inorganic light emitting diodes in comparison with representative inorganic spintronics devices. We also point out acute problems that need be resolved before the young field of organic spintronics can mature.

A. Introduction

Organic materials are promising for spintronic applications mainly because of the expected long spin relaxation time of spin polarized carriers. This results from the small spin orbit coupling (SOC) related to the light element building blocks of the organics[1]. Also the organic materials flexibility, low cost production, and unlimited versatility of chemical synthesis makes *organic spintronics* a promising alternative to conventional inorganic spintronics[3,4]. Spin-polarized transport characterized by giant magnetoresistance (MR)[5-9] was first demonstrated in fabricated organic spin valves (OSV) in 2004, with potential spintronics applications in magnetic random access memory[10-16]. This achievement has triggered plentiful of additional experiments using various organic spintronics devices, with the aim to prove spin injection from metallic ferromagnet electrodes into organic semiconductors. The present review summarizes the milestones in the field of organic spintronics devices that have occurred during the first decade of research in the field, in comparison to similar advances in the field of inorganic spintronics.

A.1 Spin injection in spintronics devices

Figure 1a shows the giant MR concept of one of the generic spintronics devices dubbed *spin-valve*. The device consists of a non-magnetic spacer sandwiched between two ferromagnetic materials (FM1 and FM2)[8,9,17,18]. A charge carrier injected from FM1 with spin sense aligned parallel to the magnetization direction of FM2 experiences *low resistance*; this is the 'parallel' alignment. In contrast, for the 'anti-parallel' configuration where the injected electron spin sense is aligned opposite to the FM2 magnetization direction, the injected charge carrier experiences *high resistance*. The switch from low resistance to high resistance (and vice versa) is induced by sweeping an external magnetic field, *B* upward (and downward) and led to the original name of this device. In OSV devices the non-magnetic spacer is a pristine organic semiconductor.

Important prerequisites for working spintronics devices using semiconductors as an intermediate layer are: spin injection, spin diffusion and spin detection.

At the present time there are three main spin injection methods into semiconductors. These are: electrical spin injection from FM electrodes, spin current induced by spin waves in FM layers, and spin diffusion from optically excited FM (or from direct band gap semiconductor).

(1) Electrical spin injection was discovered first and subsequently applied in inorganic and organic spintronics devices; most organic spintronics devices discussed in this review belong to the electrical spin injection category. When a FM metal is attached to a non-magnetic semiconductor, then upon application of a bias voltage electrons (or holes) with preferred spin polarization are injected into the semiconductor layer. This happens because of the different density of states of minority and majority carriers at the Fermi-level of the FM injector. This property is known as spin polarization capability, P, of the FM and is crucially dependent on the FM surface properties. The usable electrodes for spin injection may be: itinerary FM metal (such as Fe, Co, NiFe), half metal (such as $La_xSr_{1-x}MnO_3$; LSMO)[19,20], organic ferromagnet (such as V(TCNE)x)[21], electrode based on the effect of Coulomb blockade[22], or spin filter (such as EuS[23], MgO or organic molecular radicals[24-29]). Some of these spin injecting electrodes have been successfully used in OSV devices for studying the device performance (see section B).

(2) "Spin pumping" by spin waves: spin waves (or magnons) in FM may be activated by the process of ferromagnetic electron resonance (FMR). When the induced spin waves propagate to the FM/nonmagnetic interface, the magnons may be either absorbed or reflected at the interface. This, in turn creates a pure 'spin current' in the non-magnetic layer having spin sense parallel to the magnetization direction of the FM material under the resonance conditions[30]. The greatest advantage of 'spin pumping' is circumventing the 'impedance mismatch' that exists in the electrical spin injected method, which does not allow efficient spin

injection from a FM metal having low resistance, into a semiconductor with high resistance[31-34]. We note that spin pumping into organics was recently demonstrated by Ando *et al.*[38] and opened up a new generation of organic spintronic devices.

(3) Optical spin injection: This method may be applied to direct gap semiconductors or FM metal in contact with an overlayer of non-magnetic material. Due to the relatively strong SOC in inorganic semiconductors, circularly polarized light absorption can photo-generate an unbalanced hot electron density of spin up and down in the conduction band, thus generating a spin current (e.g. in n-GaAs)[37,38]. Consequently the proximity to an organic semiconductor overlayer may generate spin current in the latter. Similarly, optical absorption of light in a FM metal can generate spin current into a non-magnetic overlayer because of the difference in the density of hot minority and majority photogenerated carriers in the FM film.

We also mention in passing other approaches for achieving spin polarization in a semiconductor, such as high field polarization at low temperature in an organic diode subject to strong magnetic field[39], temperature gradient (spin-Seebeck) in NiFe/Pt systems, and magnetic tunnel junctions, etc.[40-45]. However the electrical injection and 'spin pumping' techniques are the main methods used to generate spin polarized current in semiconductors, and have been successfully applied also in organic spintronics devices. We note in passing that the next advance in the field of organic semiconductors may involve the optically induced method for spin injection.

A.2 Spin detection in spintronics devices

As for the spin detection, conventional spin detection is still based on electrical methods such as magneto-resistance (MR). When investigating the MR(*B*) response of devices with two FM electrodes (one for spin injector, and the other for spin analyzer), by sweeping the external magnetic field as a function of bias voltage, spacer thickness, and temperature, injected spin aligned carriers may be deduced. However, this approach cannot distinguish between spin diffusion inside the non-magnetic interlayer and direct tunnelling between the two FM electrodes, where the non-magnetic interlayer plays a minor role. Therefore, the non-local measurement technique known as the 'Hanle' effect is traditionally used to prove spin injection into and spin transport through the organic interlayer[46]. However, whether a spin preserved hopping mechanism in the organic layer can show the Hanle effect is still under debate[47]. In any case we note that the Hanle effect was conclusively shown in inorganic spin valves, and taken as evidence for spin aligned carriers[48].

Studies of muon spin rotation (μSR)[49] and two-photon photoemission[50] have provided two additional methods for detecting spin polarized carriers in organic semiconductors. Both techniques have shown high efficiency spin polarized charge carrier injection from the FM electrodes into the organic layer, with a polarization that is maintained throughout the entire organic layer (~few tens of nm thick). We note that local magneto-optical-Kerr effect (MOKE) or Faraday rotation measurements have been successfully applied to inorganic semiconductors to investigate spin accumulations, such as the Spin Hall effect[51]. Also using the pump and probe technique, the time dependence of spin polarization photo-generated by light absorption has been investigated in inorganic semiconductors, directly providing the spin relaxation time[52,53]. Alas, it is doubtful that these optical detection techniques could be adapted to organic systems because of the weak SOC that is a prerequisite for optical detection.

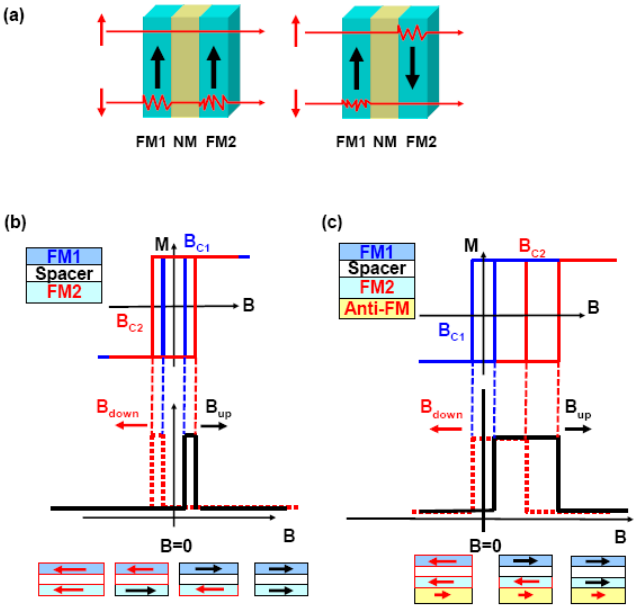

Fig. 1 (a) Explanation of the giant magneto-resistance effect: spin-dependent electron scattering that depends on the relative alignment of the ferromagnetic electrode magnetization direction. (b) Schematic geometry of "Type A" spin valve. The parallel or anti-parallel magnetization alignment is obtained by the hysteric effect of the two ferromagnetic electrodes. Black (red) arrow presents the direction of the sweeping magnetic field. Bc_1 and Bc_2 are the coercive fields of the ferromagnetic electrodes. (c) Schematic geometry of "type B" spin valve. Different from type A, the anti-parallel magnetization configuration can be obtained here by the magnetic coupling between the bottom electrode and anti-ferromagnetic layer underneath it.

A.3 The organic spin valve device

Figures 1b and 1c illustrate two types of spin valve devices that are routinely used in spintronics and their corresponding MR(*B*) response when sweeping the external magnetic field strength up, and then down. Type A configuration is the 'natural' spin-valve that has been widely used in organic spin-valves since it emerged[11]. The device is composed of two FM electrodes, where a non-magnetic interlayer is placed in between (Fig. 1b). In order to change the magnetization direction alignment of the FM electrodes from anti-parallel to parallel and vice versa upon sweeping *B*, the coercive fields (Bc) of the FM electrodes should be different from each other. Using this configuration the device resistance changes twice upon sweeping the field; this occurs at Bc_1 and again at Bc_2 (see Fig. 1b). Type B configuration includes an anti-ferromagnetic (AFM) layer underneath the bottom FM2 electrode; in this case the device resistance exhibits an abrupt change at the coercive field Bc_1, and at $B_0=J\pm Bc_2$, where J is the anisotropy exchange coupling between the two magnetic layers at the device bottom (see Fig. 1c). For type B spin-valve the coercive fields of the two FM electrodes need not be different from each other. Therefore type B spin-valve

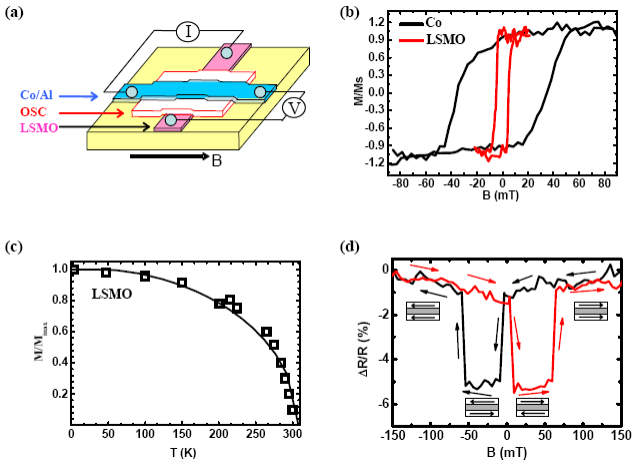

Fig. 2 (a) "Type A" prototype organic spin valve. The organic semiconductor (OS) is sandwiched between two FM electrodes; these are Co and LSMO having different coercive fields. The magnetic field (B) is applied in-plane. (b) Magnetic hysteresis loops of the Co and LSMO electrodes, obtained by MOKE measurements. (c) Temperature dependence of the LSMO electrode magnetization that indicates the FM Curie transition temperature ~307K[11]. (d) Typical MR(B) hysteresis response in a C_{60}–based OSV device measured at 10K[118]. The red (black) line represents measurements done with increasing (decreasing) B. The anti-parallel (AP) and parallel (P) configurations of the FM magnetization orientations are shown in the insets at four different magnetization alignments. The electrical resistance of the device is higher when the magnetization directions of the FM electrodes are parallel to each other. Based on ref. 118.

is more applicable for room temperature inorganic magnetic tunnel junctions (MTJ)[54,55].

Figure 2a shows the general configuration of an *organic* spin-valve using type 'A' structure. The active interlayer is made of an organic semiconductor having thickness d=10-100 nm that is placed as a spacer interlayer between the two FM electrodes having different coercive fields, as measured using the MOKE (Fig. 2b). The top electrode (FM1) is usually a hard FM (e.g. cobalt with Bc(Co) ~40mT) deposited by thermal or e-beam evaporation, having spin polarization degree (P1~30%) that is nearly independent of temperature[11]. The half-metal LSMO is usually epitaxially grown on $SrTiO_3$ substrate, and has been chosen to be the bottom FM electrode (FM2) in many OSV devices. LSMO is a soft ferromagnet (Bc(LSMO) ~5mT) that is air-stable, with Curie transition temperature, Tc=307 K, and a high spin polarization degree (P2≈98%) at cryogenic temperatures. Alas P2 strongly decreases with temperature and diminishes at ~300K[15] (Fig. 2c). The OSV resistance, R, should depend on the relative magnetization orientations of the two FM electrodes, dubbed as R_P and R_{AP} for the respective parallel and anti-parallel magnetization alignments. The figure-of-merit of a "normal" spin-valve (where $R_P<R_{AP}$) is defined by its maximum MR value within the MR(B) response, which is given by the relation $MR_{max}=(R_{AP}-R_P)/R_P$; Fig. 2d shows MR_{max} of ~6% obtained in an OSV at 10K. In many OSV, however, $R_P>R_{AP}$[11]; and therefore in the equation for MR_{max} it is customary to replace R_P by R_{AP}.

The first giant magnetoresistance (GMR), defined here as originating from spin injection and transport through the organic

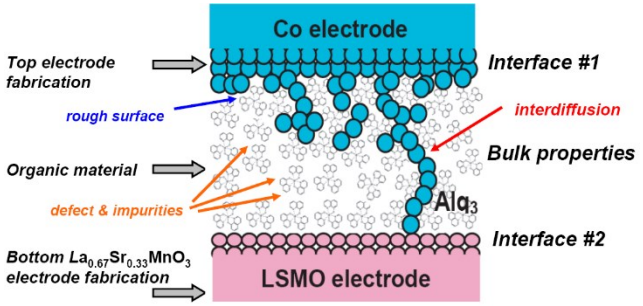

Fig. 3 Schematic of a 'real' organic spin valve device, showing the acute problems such as rough Co interface, inter-diffusion or metallic inclusions, defects and impurities

interlayer in an OSV, was achieved in 2004 using the small organic molecule Tris(8-hydroxyquinolinato)aluminium (Alq_3) for the organic interlayer[11]. Subsequently, GMR has been obtained in numerous OSV devices with organic interlayers based on small molecules (e.g. Pentacene, Rubrene, N,N'-bis (1-naphtalenyl)-N,N'-bis (phenyl) benzidiane (α-NPD), 4,4'-bis99-(ethyl-3-carbazovinylene)-1,1'-bipheny (CVB), Copper(II) phthalocyanine (CuPc), C_{60}) and π-conjugated polymers (e.g. Poly(3-hexylthiophene-2,5-diyl) regioregular (RR-P3HT), poly(dioctyloxy) phenyl vinylene (DOO-PPV)), as thick films and thin tunnel junctions, which confirm this discovery[10,14,16,50,57-70]. Many of the follow-up studies have been focused on achieving GMR at low bias voltage and high temperature (However Graphene spintronics[71-73] is not included in this review. In spite of the fact that Graphene contains only carbon atoms with weak spin orbit coupling [74,75], it has a perfect crystalline structure, with robust electronic transport properties[76], similar to inorganic materials, and in contrast to the disordered organic films discussed here). In the present contribution we review milestones in the field of OSV device fabrication, acute problems, and significant efforts to enhancing the OSV device performance (Section B). These are sorted in sections that are focused on achieving high GMR figure of merit, room temperature operation, and multi-function OSV.

B. Enhancing the performance of organic spin-valves

B.1 Acute problems in organic spin-valves fabrication

As seen in Fig. 3, the conventional OSV is composed of three layers: bottom FM1 electrode (e.g. LSMO), organic semiconductor spacer, and top FM2 electrode. This configuration includes two FM/organic interfaces, namely FM1/organic and FM2/organic. Both interfaces play an important role in the performance of the OSV device[68] since they are responsible for spin-injection and spin detection, respectively. In general, organic/metallic interfaces have been extensively studied in relation with various optoelectronic devices (such as OLEDs), using standard surface characterization methods such as scanning tunnelling microscopy, X-ray photoemission, ultraviolet photoemission, etc.[77-85]. In parallel, it has been an elusive goal to understand spin injection into organic semiconductors through FM/organic interfaces[86-89]. The main reason for the inability to obtain spin injection through such interfaces is the so-called 'resistance mismatch' between the metal

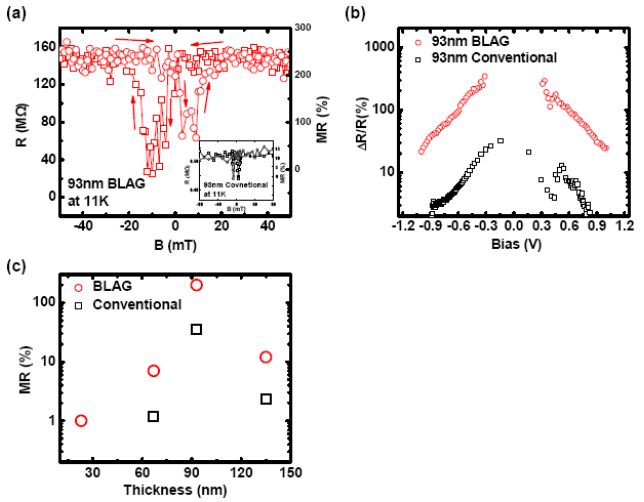

Fig. 4 (a) MR(*B*) response of a BLAG Alq_3 OSV measured at bias voltage -0.5V and 10K. For comparison the inset shows the MR(*B*) response of a conventional Alq_3 OSV obtained at the same effective thickness and bias voltage. (b) MR(V) response of a BLAG and conventional OSVs measured with Alq_3 thickness of 93 nm. (c) Same as in (b) but for MR(d) response measured at 0.5 Volt. Based on ref. 112.

electrode (small R) and the organic semiconductor (large R), which does not allow substantive spin injection from a FM into a semiconductor[32-35].

Another acute problem is the existence of metal inclusions that impair spin injection in many organic systems[11,90]. Due to the diffusion of atoms belonging to the top metal electrode during the fabrication process where 'hot' atoms are involved, the gap between FM1 and FM2 decreases substantially to the point that spin-polarized tunnelling between the FM electrodes may take place, resulting in tunnelling magnetoresistance (TMR) as an alternative to the GMR effect in OSV. The mechanism for spin injection and transport (TMR or GMR) inside the organic layer is still intensely debated[11-16,56-67]. The hot atoms diffusion problem may be circumvented in horizontal organic spin valves[69,70]. However horizontal organic spin valves should have miniature gaps of the order of 50 nm or less, which is dictated by the small spin diffusion length in the organics. Small gaps are difficult to fabricate because the resolution of the most advanced e-beam lithography techniques at present is ~ 30 nm[48]. Other effects such as anisotropic magnetoresistance in the FM electrode, anisotropy tunnelling magnetoresistance[91], interface magnetoresistance[29], and fringe field of FM electrodes[92] have also been also mentioned as disturbing mechanisms that may prevent GMR in OSV. We note that the clearer experiment that proves spin injection and spin transport, namely the Hanle effect, so far has not been observed in OSV[47,48]. It is also worth mentioning that the spin transport mechanism in the organic interlayer (for example spin preserved hopping) is not very well understood at present, and is far more complicated compared to the traditional spin transport in inorganic spintronics devices.

When an organic layer is deposited onto a metallic film by evaporation or spin casting from solution, the organic semiconductor usually forms a disordered film having ample vacancies and other defects[93-97]. Under these conditions conventional transport models which have been used to describe carrier/spin transport in single crystal inorganic materials[98], may not fit this complex situation in OSV[99-104]. For instance, band transport does not fit this situation since it requires highly purified molecular crystals and Bloch wave-functions[105]. In contrast the space-charge-limited current (SCLC) for bulk-limited charge conduction[106-108], Fowler-Nordheim tunneling (FN-tunneling) and Richardson-Schottky (RS) model of thermionic emission for injection-limited conduction[109] are the proper mechanisms used in most organic based devices (i.e. OLEDs and Organic field-effect transistors); however we note that spin transport in OSVs is still unsettleed[110]. Usually spin-preserved hopping between localized molecules was considered for spin transport in the organic layer, but there is still no consensus. Although the existence of long spin relaxation time in organic materials has been verified by electrical[49,111] and optical[50] measurements, still carrier mobility in organic semiconductors is quite low (varies from 10^{-5} to 0.5 cm^2/volt-sec)[12,102]due to the hopping type transport. Consequently the spin diffusion length, *Ls* which is determined by the relation $Ls \propto \sqrt{D\tau}$; where *D* is the carrier diffusion coefficient that is proportional to the mobility, and τ is the spin relaxation time[98], is relatively small (of order of tens of nm)[61,102,111] compared to conventional inorganic materials (e.g. GaAs, with *Ls* up to hundreds of μm[4]). The small *Ls* may diminish the use of organic semiconductors in spintronics applications. Improving the OSV performance by enhancing *Ls* has been therefore a primary goal of the field of organic spintronic.

B.2 Improving the magnetoresistance figure of merit

B.2.1 Interface engineering for spin injection/detection

In order to achieve large MR value, it is imperative to improve the efficiency of spin injection (detection) into (from) the organic layers. In the last decade the MR value in inorganic spin-valves has been substantially enhanced by improving the FM/spacer interfaces[54,55]. Mimicking the improved performance of inorganic spin-valves, a similar approach has been tried for preventing the inter-diffusion of hot atoms into the organic layer during the fabrication stage, by inserting a buffer layer between the FM electrode (FM2) and the organic interlayer. This was dubbed 'interface engineering' of OSV devices[68].

Rather than evaporating the cobalt atoms (FM1) directly from the hot Co metal crucible source, as has been routinely done in conventional OSV device (Conv-OSV) fabrication, Sun *et al* used a buffer-layer assisted growth method (BLAG) method. In this technique they first deposited at low temperature several monolayers of high density cobalt nanodots onto the organic film, followed by normal Co evaporation[112]. In this method the hot Co atoms form aggregates with the pre-deposited Co nanodots rather than penetrating into the organic layer. Thus the interdiffusion of the deposited Co atoms into the organic film could be suppressed, and consequently a large MR (~200%) value was obtained at 10K (Fig. 4a). With the same Alq_3 interlayer thickness, the MR value of Conv-OSV was measured to be only ~12%, which is substantially lower than the MR obtained with the OSV fabricated by the BLAG method (dubbed BLAG-OSV). The MR voltage dependence in Fig. 4b shows that the obtained MR for the BLAG-

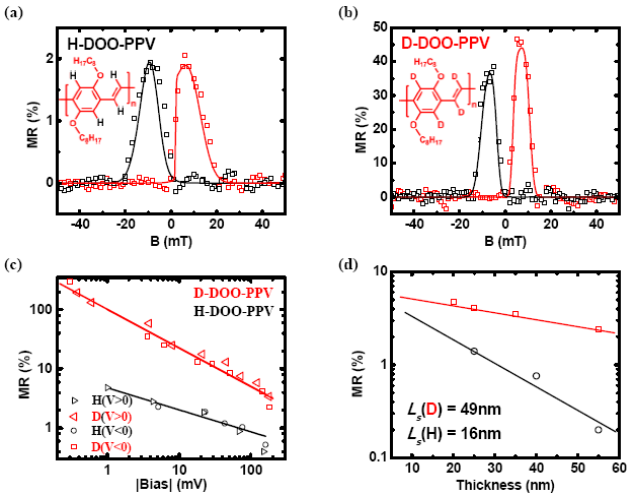

Fig. 5 (a) and (b) Comparison of MR(*B*) response obtained for H- and D-DOO-PPV OSV devices at 10K, respectively. (c) and (d) MR(V) and MR(d) dependencies for the two OSV devices. Based on ref. 117.

OSV devices is much larger than that of Conv-OSV at all voltages. Fig. 4c shows the obtained MR values of the two OSV types as a function of the Alq_3 interlayer thickness. An enhanced MR is observed for all thicknesses when the BLAG method was used. The increase in the MR at ~ 93 nm in both BLAG-OSV and Conv-OSV is surprising, because in many OSV devices the obtained MR decreases with the organic layer thickness. Such a behavior, however is expected if an ill-defined layer is formed that results from the Co inclusion even in the BLAG OSV[90,112].

Yoo *et al.* used an organic FM film as the top electrode (FM1) to fabricate an 'all organic spin valve'[21]. The organic FM could be grown as a thin film by low-temperature (40K) chemical vapor deposition method. At this low temperature deposition the interdiffusion of the organic FM into the organic semiconductor layer is significantly suppressed. The obtained MR value however was ~2% at low temperature, which is significantly lower than that obtained in standard, Conv-OSV. The reason for the low MR value in the 'all organic OSV' may be due to the lower spin polarization degree of the deposited organic FM electrode.

Dediu *et al.* incorporated an inorganic insulator (Al_2O_3) between the top Co electrode (FM1) and organic layer in order to slow down the interdiffusion, and improve the stability of the OSV device[113]. However, the suppressed interdiffusion was achieved at the expense of losing some spin polarization injection capability from the Co electrode; thus the MR value of such Al_2O_3-OSV device was ~10% at low temperature. Barraud *et al.* fabricated a nanoscale LSMO/Alq_3/Co OSV tunneling device[114]. The nano-indent in the LSMO/Alq_3 layer was realized by Conductive-Atomic Force Microscopy that allowed control over the organic tunnel barrier thickness. Subsequently the obtained nanohole was filled with cobalt that formed the top electrode (FM1). This nano-fabrication led to a nano-size magnetic tunnel junction (MTJ), which exhibited up to 300% MR at low temperature. The authors concluded that the high obtained MR in the nano-size OSV device may be due to the hybridization between the organic layer and bottom FM electrode (FM2); this hypothesis was later supported by two-photon photoemission measurements[115].

B.2.2 Enhanced spin diffusion in the organic interlayer

From the magnetoresistance equation[11,17,116]: $MR \propto 2P_1P_2\, e^{(-d/Ls)}/(1+P_1P_2)$ (where P_1 and P_2 are the polarization degrees of the FM electrodes, and d is the organic interlayer thickness), it is clear that the MR in OSV depends on the thickness and spin diffusion length of the organic interlayer. Therefore to improve the figure of merit there is the need to optimize L_S in the organic material[102]. Organic semiconductors are composed of light elements that possess weak SOC. Consequently the spin-relaxation time of the injected carrier should be long. However in the absence of strong SOC the hyperfine interaction (HFI) becomes the most significant factor in limiting L_S. Consequently the spin diffusion length, and in turn the MR may be controlled by manipulating the nuclear spins of the organic spacer atoms. Using the chemical versatility of organic semiconductors, we recently fabricated and compared the spin responses in OSV devices based on π-conjugated polymers made of protonated, H-, and deuterated, D-hydrogen that have weaker HFI strength[117].

Figure 5a shows a typical MR(B)=(R(B)-R(AP))/R(AP) response of an OSV device based on poly(dioctyloxy) phenyl vinylene (H-DOO-PPV) polymer obtained at T=10 K and bias V=10 mV. The MR decreases sharply with the bias voltage, V (Fig. 5c) and organic layer thickness, d (Fig. 5d). The MR decrease with d is caused by the finite L_S of the injected spin aligned carriers. To test the role of the HFI, the backbone PPV protons in the DOO-PPV polymer were replaced by deuterons; this isotopic-exchanged polymer was dubbed D-DOO-PPV (see Fig. 5b, inset for its chemical structure)[107]. The deutron has reduced magnetic moment relative to that of the proton, and therefore weaker HFI constant, a. Typically the HFI coefficient is $a/g\mu_B$~3 mT for protons and ~0.5 mT for deuterons in polymers such as DOO-PPV (where g≈2 is the polaron g-factor and μ_B is the Bohr magneton)[108]. Figures 5b to 5d show that the obtained MR for OSV devices based on D-DOO-PPV is indeed much larger than that of devices based on naturally abundant H-DOO-PPV. Fitting the MR(d) response with an exponential function, $MR \propto \exp(-d/L_S)$[11] (Fig. 5d), it was found[107] that L_S of D-DOO-PPV is ~50 nm compared to L_S ~16 nm in regular H-DOO-PPV. It was concluded that the increase in Ls results from the smaller HFI a in D-DOO-PPV, and this provides evidence that the major spin relaxation process that limits the spin diffusion length in π-conjugated polymers is indeed the HFI.

In addition the MR in OSV strongly decreases with the bias voltage, V as shown in Fig. 5c. It is not clear whether the decrease with V is due to surface-electrode effect, or it originates within the bulk of the organic spacer. Figure 5c shows that the MR decrease with V cannot be entirely due to the organic interlayer, since it occurs in OSVs based on *both* isotope-rich polymers. Interestingly Fig. 5c also shows that at small bias voltage (~0.3 mV), the MR response reaches a value of 330% by optimizing the D-DOOPPV polymer thickness. This large MR value is in fact in agreement with the largest MR achieved in OSV so far in miniature OSV[114].

Another attempt to achieve higher MR is using C_{60} based OSV devices fabricated with LSMO and Co ferromagnetic electrodes[118].

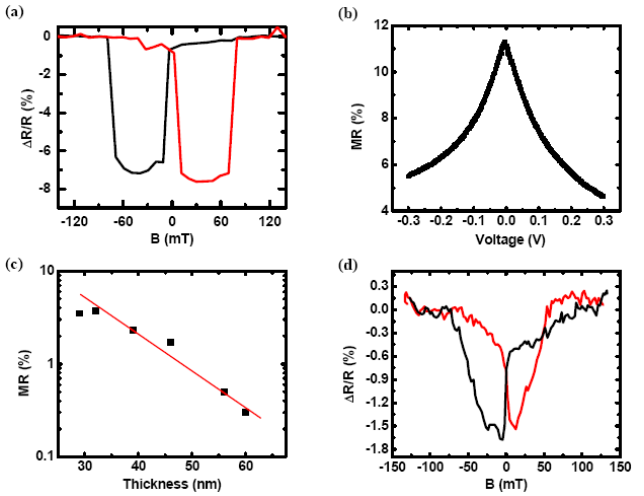

Fig. 6 MR(B) response (a), voltage dependence (b) and thickness dependence (c) of the MR for C_{60}-based OSV device at 5K. (d) MR(*B*) response of ^{13}C-rich C_{60} OSV device at the same bias voltage that shows the isotope effect. Based on ref. 118.

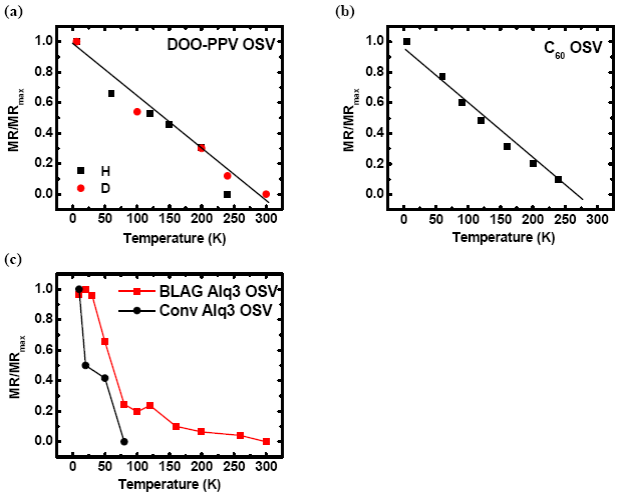

Fig. 7 MR temperature dependence for OSVs based on (a) H- and D- DOO-PPV, (b) C_{60}, and (c) BLAG and conventional Alq_3. Based on ref. 112, 117, 118.

Unlike the previous example of OSV based on a DOO-PPV polymer interlayer, in which the HFI played a major role in limiting L_S, here the buckeyball C_{60} molecule is composed of 60 carbon atoms, of which 98.9% are the natural abundant ^{12}C isotope having spinless nucleus, and thus zero HFI. Consequently it has been assumed that the spin diffusion length in fullerenes would be relatively large, resulting in a potential high MR in fullerene-based OSV devices. Figure 6a shows typical MR(*B*) response of a C_{60}-based OSV device fabricated with the usual four-layer configuration of LSMO/C_{60}(35nm)Co/Al. The MR response here is 'text-book' example; it is quite sharp with two well defined resistance jumps at the FM2 and FM1 coercive fields. Figure 6c shows the MR(*d*) thickness dependence for d>30 nm measured at 10 K. An exponential fit MR(d)∝exp(-d/L_S) yields a relatively short diffusion length, L_S~12 nm. Surprisingly, the spin diffusion length is not as long as expected in C_{60}-based OSV. We note, however that for d<30 nm, a morphology-related disorder that originates from the C_{60} nano-crystalline grains embedded into an amorphous phase of the C_{60} film may interfere with the spin transport[118]. C_{60} films are quite robust and thus Co atoms inter-diffusion into the organic layer is suppressed [119]. Thus Co inclusions cannot explain the small spin diffusion length here; we are thus left with the nanocrystalline grains as the underlying mechanism for the small L_S value. In fact it was found that the C_{60} nanocystalline grain size increases with the film thickness up to d~35nm, where it stays constant with further increase in d. Moreover it was concluded that the main spin relaxation process in C_{60} occurs in the nanocrystalline grains[108]. This explains the MR increase with d that was obtained up to d~35 nm[108]. For d>35 nm the spin relaxation rate is constant, and therefore Ls could be measured using the usual exponential fit as in Fig. 6c.

In order to elucidate the role of the HFI in the C_{60} based OSV, we show in Fig. 6d a typical MR response of a ~25% ^{13}C-rich C_{60} OSV obtained at low temperature. ^{13}C isotope has a nuclear spin ½ and thus a sizable HFI constant $a/g\mu_B$~1 mT. It is not surprising therefore that the obtained MR value is substantially smaller compared to that of OSV based on naturally abundant C_{60} (Fig. 6a), most probably due the stronger HFI in the ^{13}C isotope-rich fullerene. This demonstrates the important role of the HFI in limiting the OSV figure-of-merit. Since the HFI is small in natural C_{60} a likely mechanism for the short spin diffusion length in C_{60} OSV could be the SOC. The fullerenes are strongly curved, and this allows significant hybridization between their π and σ electrons. Recent calculations have estimated the SOC coefficient in C_{60} to be ~1 μeV[120]. This is a relatively small value, but is larger than the HFI in this molecule, and thus may be the limiting factor in determining the spin diffusion length in C_{60}-based OSV devices.

B.3 Room Temperature Operation

Compared to inorganic based spin-valve devices, for which tunneling MR (TMR) larger than 600% was achieved at room temperature[121,122], the maximum GMR value of OSV devices at room temperature was reported to be ~2%[123-125]. Thus the performance of OSV devices at room-temperature needs be substantially improved. The first obstacle for higher MR at room-temperature is the drastic decrease of the degree of the polarization related to the LSMO FM electrode at room temperature (Fig. 2c); this is due to its relatively low Curie temperature (Tc=307 K). Although at room temperature LSMO still shows decent ferromagnetic properties, the efficiency of spin injection determined by the FM spin polarization degree at the film's surface may be greatly suppressed even at 300 K, and thus no decent GMR can be obtained[113]. In fact all observed high MR values in OSV have been achieved at low temperature, using the "magic" LSMO half-metal electrode since it exhibits ~98% spin polarization at 10K[19,20]. Therefore an alternative hole injecting FM electrode having higher Tc has been sought. We note that the magnetization of the cobalt FM cathode only slightly decreases with increasing temperature up to 300K, indicating that the spin polarization degree of the cobalt electrode does not directly account for the low MR in OSV at RT. However its polarization degree is relatively small.

Figure 7a shows the MR(T) temperature dependence for H- and D-DOO-PPV OSV devices. Taking into account the similar polymer structure, same ferromagnetic electrodes, and configurations of both OSV devices, their similar temperature dependent MR(T) response shows that is not affected by the HFI. Figure 7b shows MR(T) in C_{60}-based OSV that exhibits a similar decrease with the temperature as that of DOO-PPV-based OSV devices. Fig. 7c shows MR(T) in a BLAG-OSV and Conv.-Alq_3-based OSV devices that also show similar MR(T) dependence as most OSV devices. Considering the similar MR temperature dependence of OSV devices from polymers, fullerenes, and small molecules, we conclude that the spin injection from LSMO electrode plays a crucial role in determining the MR(T), rather than the organic material properties. Therefore, in order to achieve decent MR value at room temperature, the bottom ferromagnetic LSMO electrode needs be replaced by a FM electrode having a weaker polarization degree P(T) dependence, but that still possesses high polarization degree.

Modification of the FM electrode for efficient spin injection into organic material at RT has been achieved in organic *magnetic tunnel junctions*. Santos *et al.* introduced a very thin Al_2O_3 buffer layer (0.2 nm to 1.0 nm) between Co and Alq_3[126]. As a result significant TMR (5%) was measured at room temperature. An interfacial dipole layer between the organic and metal electrode was believed to improve the spin-polarized tunneling behavior. Alternatively, Szulczewski *et al.* optimized the OSV fabrication procedure by using MgO spin filter instead of Al-O tunnel barrier between Alq_3 and FM2 (CoFeB in this case) bottom electrode[127]. The obtained TMR value reached 12% at room temperature. Although reasonable room temperature TMR values was observed in these devices, GMR, where the injected spin aligned carrier *diffuse* to the opposite FM electrode rather than tunnel through the organic interlayer, is still quite small at room temperature.

Recently, Zhang *et al.* chose a Fe_3O_4/Al-O hybrid bottom electrode (FM2) that replaces the LSMO in the OSV architecture, and obtained ~5% GMR in C_{60}-based OSV devices at room temperature[128]. By analyzing the MR dependence on the C_{60} thickness, spin diffusion length of about 110 nm was experimentally extracted at RT under optimized fabrication condition. Although further investigations need be done to understand the spin transport mechanism (such as in spin-conserved hopping) in C_{60} and spin injection/detection efficiency at the FM/C_{60} interfaces; these results, for the first time, illustrate the possible application of OSV devices at RT with MR that is comparable to that in the inorganic counterparts.

The limitation of spin polarization in FM electrodes, and the unexpected short spin diffusion length in most organic materials can be circumvented in another type of MR (dubbed organic magnetoresistance, or OMAR) which exists in non-magnetic organic diodes[129-131]. OMAR originates from the spin interaction of the injected electrons and holes in the organic diode, and may reach MR value of 60% at RT[130]. Recently it has been reported that OMAR reached 2000% at room temperature, in a 1D organic based device[132]. We note, however that OMAR response is controlled by the internal spin interactions of the injected carriers in the organic active layer, rather than by FM electrodes. Apparently OMAR is enhanced when the organic layer is subjected to UV light illumination, or electron beam bombardment[133]. Consequently, OMAR value at room temperature is difficult to control, and may be even related to the device operation history. Moreover OMAR is a passive effect; namely, its value corresponds directly to the magnetic field strength. In addition it does not exhibit the remnant high and low resistance states at zero field, as is the case for the MR in conventional spin-valves. Interestingly, Wang *et al.* discovered a new approach to obtain a remnant OMAR value in organic diodes by introducing a 'fringe field effect' related to FM electrodes that modifies the device architecture[134]. The obtained fringe field effect in OMAR is due to the unsaturated magnetization state of the bottom FM electrode (separated from the organic layer by a thin layer of PEDOT or ITO). The fringe field adds to the external magnetic field, i.e. $B_{tot}=B_{fringe}+B_{ext}$ and thus gives a remnant OMAR at $B_{ext}=0$, similar to a spin-valve response[135,136]. We also note that the remnant OMAR due to the 'fringe field effect' may reach substantial value of ~12% at room temperature.

B.4 Multi-functional organic spin-valve devices

Organic spintronics devices have an important advantage over the inorganic counterparts that is the organic materials in the devices are not passive, but instead they emit light, are flexible and can be doped in situ. These unique properties of the organics have been taken into account for engineering spintronics devices having multi-functional activities[137,138,139].

B.4.1 Changing the MR sign in organic spin-valves

Schulz *et al.* discovered that the spin sense of extracted charge carriers from a FM/organic interface, and the obtained MR sign can be tuned by inclusion of a thin interfacial layer of the polar material (LiF)[140]. The underlying mechanism of this interesting phenomenon is the electric dipole moment brought about by the LiF buffer layer, which shifts the highest occupied molecular orbital (HOMO) level of the organic with respect to the Fermi energy of the FM electrode (in that case, Co). Consequently a band having an opposite spin sense is reached at the FM electrode surface that dominates charge-carrier extraction; this results in MR sign change for the OSV device[141]. We note, however that the resulting OSV is still a passive device. Using this concept a multi-memory state device (namely three states: "+1", "-1" and "0") may be engineered rather than the conventional OSV devices that have only "0 and "1" states. This idea was recently introduced in inorganic magnetic tunnel junctions, by adding a ferroelectric layer (Lead Zirconate Titanate ($PbZr_xTi_{1-x}O3$)) between two FM electrodes[142]; this device configuration was also tried recently with OSV[143].

B.4.2 The spin OLED device

Another example of multi-functional OSV is the recently announced bipolar OSV, in which both current and electroluminescence (EL) intensity are controlled by an external magnetic field[144,145]. The general structure of the bipolar OSV is shown in Fig. 8a. It has a similar structure to that of a conventional unipolar OSV shown in Fig. 2a, except that both spin-aligned

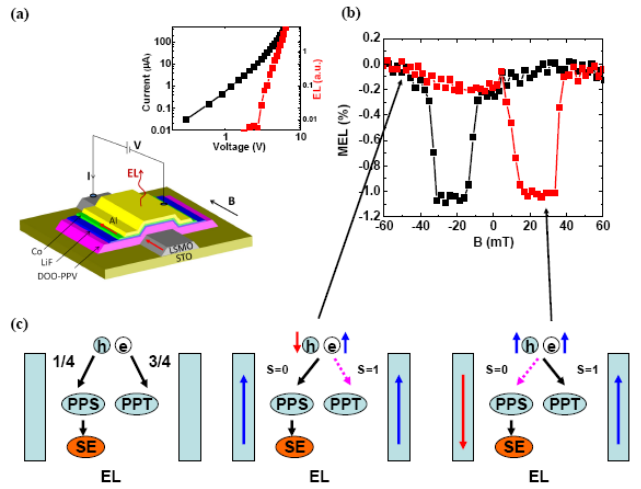

Fig. 8 (a) Schematic of bipolar organic spin valve device. The inset shows the I-V and EL-V characteristics on a logarithmical scale; bipolar injection turns on at 3.5 Volts. (b) Typical MEL(*B*) response measured at 10K and 4 Volt. (c) Bipolar organic spin valve device operation under parallel and anti-parallel FM electrode magnetization alignment; the arrows point to the corresponding electro-luminescence intensity in the MEL(*B*) response. Based on ref. 145.

electrons and holes are injected into the organic interlayer. This allows EL emission when bipolar injection occurs at bias voltage larger that the turn-on voltage. However, with D-DOO-PPV as the organic interlayer (Fig. 8b, inset), the Co work function (~5 eV) hardly allows any electron injection, and this prevents bipolar injection to occur. Therefore a thin LiF layer (thickness, *d*', in the range of 0.8 to 1.5 nm) was deposited as a buffer layer between the organic layer and Co ferromagnetic electrode in order to both improve the electron injection capability and block the formation of Co inclusion. The inset of Fig. 8a shows the *I-V* and *EL-V* characteristic of the bipolar OSV that emphasizes the occurrence of bipolar injection; this leads to EL emission at bias voltage higher than the 'turn-on' voltage of V~3.5V, where a bipolar space-charge limited current density conditions are reached in the device. This prototype bipolar organic spintronics device may be viewed as a spin polarized organic light emitting diode (or spin-OLED). Similar to an ordinary OLED, electrically injected positive and negative charge carriers fuse together to form (dark) triplet (spin S=1), or (bright) singlet (S=0) excitons (Fig. 8c) that may recombine radiatively and generate EL emission. However in a bipolar spin valve device, spin polarized charge carriers alter the generated singlet to triplet exciton ratio (1:3 in regular OLED); and this, in turn, changes the EL intensity from the singlet excitons.

Figure 8c presents the working principle of the bipolar spin valve in more detail. In a conventional OLED, electrically injected holes and electrons from non-magnetic electrodes and thus that are not spin aligned, fuse together to from singlet excitons and triplet excitons at a ratio of 1:3[146]. Without the existence of heavy atoms with large SOC in the D-DOO-PPV polymer, the dark triplet excitons cannot recombine radiatively and thus do not contribute to the EL. In this case only singlet excitons are radiative. The EL intensity is therefore proportional to the singlet excitons density. When the non-magnetic electrodes are replaced by FM electrodes, the injected holes and electrons are spin-polarized to some degree; for the sake of argument we may assume here 100% spin polarization. We note that the spin sense of the injected holes is opposite to the magnetization direction of the injecting FM electrode (LSMO is considered as the hole injector), while the injected electrons have the same spin sense as the magnetization direction of the cobalt/LiF layers. Under these conditions, the formation ratio of singlet and triplet excitons is altered according to the magnetization configuration of the two FM electrodes. In the parallel (P) magnetization configuration, the injected holes and electrons have opposite spin sense, and this spin configuration enhances the singlet formation up to 50%. However for the anti-parallel (AP) magnetization configuration the spin senses of the injected electrons and holes are parallel to each other, leading to the exclusive formation of triplet excitons. Thus EL emission from singlet excitons is increased in the parallel magnetization configuration respect to the anti-parallel configuration. Consequently, by adjusting the FM electrode magnetization configuration from parallel to anti-parallel when sweeping the magnetic field, the EL emission intensity in the bipolar organic spin valve can be actively controlled. The obtained $MEL_{EX}(B)=[EL(B)-EL(AP)]/EL(AP)$ response (Fig. 8b) of the bipolar OSV is composed of a 'non-hysteretic' smooth component due to the "intrinsic" MEL diode response[130,148], and a 'hysteretic' negative MEL_{hys} component that consists of a downward jump of ~1% in the antiparallel magnetization configuration between 4 and 30 mT that follows the electrodes' coercive fields. This effect can in principle be used to detect the degree of spin polarization of the injected carriers. Furthermore, in OLEDs where both EL emission and longer wavelength electro-phosphorescence (EPH) emission can be obtained, an external magnetic field may be used to control the device EL emission color.

B.4.3 The hybrid spin-OLED device

The difficulty in achieving room temperature bipolar-OSV operation is two-fold: (a) significant OSV response is usually limited to low bias voltage (< 1 V), whereas for efficient EL (and MEL) much higher bias voltage needs be supplied (>10 V for Alq_3 based OSV), where the spin polarization injection from the FM electrodes is substantially reduced (see the MR(*V*) dependence in Figs. 4 and 5). (b) The lack of FM electrodes that can effectively inject both spin aligned holes and electrons into the organic interlayer at room temperature. The limitation of spin polarization for conventional FM electrodes at room temperature is the bottle-neck obstacle. However, inorganic spin valves, or magneto-tunneling junctions (MTJ, Fig. 1) exhibit giant room temperature TMR using spin filter barrier (MgO). Thus an alternative way that circumvents the need to find a new high spin polarization FM electrode at room temperature, is to fabricate a hybrid device that combines the properties of MTJ and OLED devices. In fact such a device was recently introduced leading to giant MR and MEL in organic devices at RT, namely in a hybrid organic/inorganic spin-OLED (dubbed h-OLED)[149]. The h-OLED device combines the advantages of inorganic MTJ device having high MR at RT that can be easily integrated to other devices, and OLED having efficient EL emission, flexibility and low production cost; these components are combined in series. This method is universal, namely can be applied to any OLED based on small molecules or

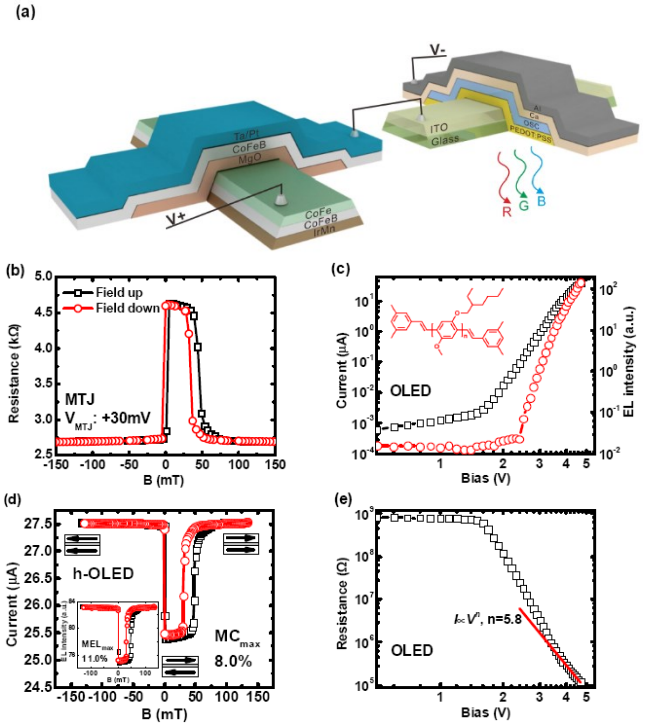

Fig. 9 (a) Schematic structure of an hybrid OLED device, including a magnetic tunnel junction (left side) and conventional OLED (right side) connected in series. The magnetic field is applied on the MTJ device component. (b) TMR(B) response of the MTJ component at room temperature. (c) I-V and EL-V characteristic of a MEH-PPV OLED. (d) MC(B) and MEL(B) responses of the hybrid-OLED device measured at room temperature. (e) Voltage dependence of the MEH-PPV OLED resistance; in the space charge limited current regime the device resistance steeply decreases with V. Based on ref. 149.

polymers, giving electro-phosphorescence (EPH) or EL emission, respectively.

Figure 9a shows the hybrid device architecture used and its operation scheme[149]. The h-OLED device contains two sections: an inorganic MTJ component and an OLED component. For the MTJ component we used MgO tunnel barrier in between CoFeB and CoFe ferromagnetic electrodes, where the CoFe electrode is deposited onto thin CoFeB layer, and IrMn layer which is an anti-ferromagnet (AFM, Fig. 9a). This type of MTJ yields the best TMR performance at room temperature (~ 50% to 600%)[54,55,121,122]. The OLED component is a traditional light emitting device composed of indium tin oxide (ITO)/hole transport layer (PEDOT:PSS)/organic semiconductor (OSC)/calcium (Ca)/aluminium (Al). The OSC layer may be based on any molecule, polymer, or polymer/molecule (host/guest) blend with high EL emission yield. During operation the h-OLED device is biased with a constant voltage, and an in-plane sweeping magnetic field, B is applied to either the MTJ, OLED, or simultaneously to both MTJ and OLED device components.

A typical TMR(B) response of the MTJ device at bias V= +30 mV and RT is shown in Fig. 9b. TMR(B) response exhibits an abrupt resistance change (of ~75%) at the coercive fields of the two FM electrodes (type B spin-valve, see Fig. 2c). Figure 9c shows the I-V and EL-V characteristic at room temperature, which are typical OLED responses. The active organic layer in the OLED is poly[2-methoxy-5-(2-ethylhexyl-oxy)-1,4-phenylene-vinylene] (MEH-PPV), of which repeat unit is shown in Fig. 9c inset. The OLED I-V response contains two voltage regimes; an Ohmic regime with constant resistance, R_2 ~600 MΩ, and a space-charge-limited current (SCLC)[107] regime ($I \sim V^n$; with n~5.8) caused by bipolar injection which generates EL emission. In this SCLC regime the device resistance, R_2 drops as a power law in V ($\sim V^{-(n-1)}$) down to ~120 kΩ at ~ 4.7 Volt (Fig. 9e). The relative small change of the resistance (~2.0 kΩ) in the MTJ upon sweeping the field seems to be insufficient for altering the OLED resistance, and in turn the EL emission, because of the large resistance mismatch between the two device components. Luckily, it was found that there is a "MR amplification" when the two components were connected in series, where the OLED non-linear I-V response in the SCLC regime effectively reduces R_2 by a large factor, n, and thus the resistance mismatch between the two device components is not as severe as anticipated for an ohmic R_2 case.

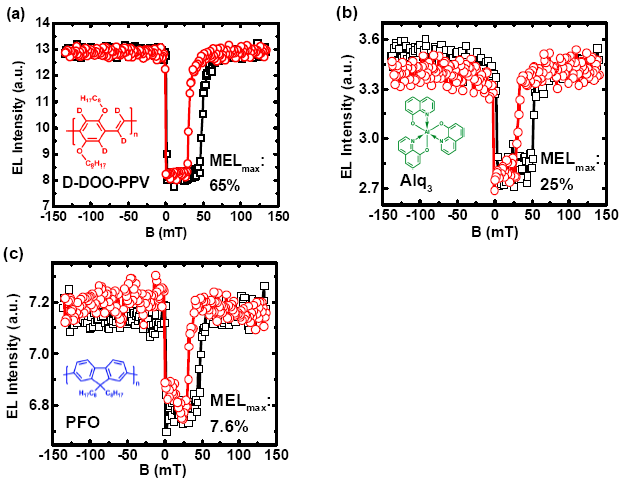

Fig. 10 MEL(B) responses of three h-OLED devices measured at room temperature. The devices are based on (a) D-DOO-PPV with red emission; (b) Alq_3 with green emission; and (c) PFO with blue emission. The D-DOO-PPV polymer repeat unit (red), Alq_3 structure (green), and PFO polymer repeat unit (blue) are shown in the corresponding insets. Based on ref. 149.

The inset of Fig. 9d shows the MEL(B) response of the same h-OLED device measured at V=4.6 Volt and RT. It is seen that the MEL(B) response follows the response of the MC(B) (Fig. 9d). There are sharp MEL increases at Bc_1 and B_0. Also the maximum MEL, MEL_{max}=11.0% is higher than MC_{max}, which may be explained by the nonlinear EL-V response (Fig. 9c). This shows that the h-OLED device may deliver substantive MEL at RT, which has been the long-sought goal of the Organic Spintronics field. In principle, the h-OLED device may be used at any temperature, with any OLED system having phosphorescence or luminescence emission (or both), based on small molecules or polymers, and thus may span the entire visible spectrum. To demonstrate this we introduced three h-OLED devices that show giant MEL at RT with emission bands in the red (Fig. 10a; D-DOO-PPV polymer), green (Fig. 10b; Alq_3 molecule), and blue (Fig. 10c; PFO polymer), and thus covering the entire visible

spectrum. In particular the room-temperature MEL(B) response of the h-OLED based on D-DOO-PPV (Fig. 10a) shows giant MEL_{max} up to ~81%[149], which is very promising value indeed.

C. Conclusions

In summary, we reviewed here a number of significant advances in the young field of organic spintronics that have occurred during the first decade of research investigations. Starting from the description of the most generic spintronics device, namely the organic spin-valve (OSV), we described the acute problems in obtaining substantial controlled giant magneto-resistance (GMR) in OSV at room temperature. We also reviewed the OSV magneto-resistance dependencies on temperature, bias voltage and organic interlayer thickness. The underlying physics that explains the temperature and bias GMR dependencies is not clear at the present time; there are conflicting models, but a conesus has not been found. The dominant process of the spin relaxation mechanism in the class of organic semiconductors is the hyperfine interaction (HFI) with the proton nucleus, since the spin-orbit coupling (SOC) is relatively small in these materials. Surprisingly, however the obtained spin diffusion length in the organics (including fullerenes that lack HFI), which may be extracted from the GMR interlayer thickness dependence is small, of the order of tens of nm.

The advantage of organics for spintronics applications is in fact also a disadvantage, since the lack of strong SOC prohibits the use of magneto-optical effects for measuring spin injection from FM electrodes into the organics[51-53]. Thus the principal method for investigating spin injection into the organic layer has been electrical, by means of the GMR(B) response. This is an elusive measurement since the 'resistance mismatch' known to exist in spin injection into inorganic semiconductors, may be applicable also to the organics [33,34]. Alas, the Hanle effect in which the MR in spin-valves changes upon the application of an additional *perpendicular* magnetic field, which in inorganic spintronics has been the compelling experiment that proves spin injection into semiconductors[46,48], has not been successfully measured in OSV as yet. To some, the lack of the Hanle effect is a cause for concern[47]; however there are other, indirect, evidences that show the occurrence of spin aligned carrier injection from FM electrodes into organic semiconductors. One such experiment is the muon spin rotation that measures the internal field strength induced by the injected carriers[49]. Another experiment is the two-photon spin injection from a FM into an organic semiconductor[50]. Both of these experiments showed conclusively spin injection. An indirect evidence for spin injection is the demonstration of spin-OLED. If spin injection would be absent in such devices then the demonstrated control of the EL intensity would not have occurred[145]. We anticipate that more experiments that prove spin injection into organic materials would be done, and that explanation of the lack of the Hanle effect in OSV would be found.

We also described some unique OSV multi-functional abilities. One such application is the spin-OLED that showed magneto-electroluminescence (MEL) up to 1.2% at low temperature[145]. The MEL value is perhaps not substantial, but the ability of injecting simultaneously both spin aligned electrons and holes is new in the field of spintronics. The physics of spin aligned carriers in the regime of space charge limited current density is novel and interesting. Another recent demonstration of organic spintronics application is the hybrid-spin-OLED that is capable of delivering 'all colors' MEL up to 80% at room temperature[149]. This device is not restricted to OLED; in fact large MEL value was also achieved using inorganic LED. There are other multifunctional applications that were not described in this review, and we anticipate other unique applications to emerge during the second decade of research in organic spintronics.

Acknowledgements: We thank L. Wojcik for the isotope-rich compounds, and Dr. Tho D. Nguyen and Dr. Fujian Wang for various experiments. This work was supported by the DOE Grant No. DE-FG02-04ER46109 (the bipolar OSV; ZVV) the NSF grant No. DMR-1104495 and NSF MRSEC grant No. DMR 11-21252, (ZVV; C60 films and OSV devices); the Israel Science Foundation Grant No. ISF 472/11 (the bipolar SCLC model; E.E.), and the US-Israel BSF Grant No. 2010135 (the spin-OLED; Z.V.V. and E.E.)

Notes and references

[a] *Department of Physics and Astronomy, University of Utah, Salt Lake City, Utah, USA. Fax: +001 8015814801; Tel:+001 8015816901; e-mail: sund@physics.utah.edu, val@physics.utah.edu*
[b] *Physics Department, Technion-Israel Institute of Technology, Haifa, Israel. Fax: + 9724 8235107; Tel: +972 48293610; e-mail: eitane@technion.ac.il*

1. W. J. M. Naber, S. Faez and W. G. van der Wiel, *J. Phys. D: Appl. Phys.,* 2007, **40**, R205.
2. Z. V. Vardeny Organic Spintronics (CRC Press, 2010), 1st ed.
3. S. A. Wolf, D. D. Awschalom, R. A. Buhrman, J. M. Daughton, S. von Molnar, M. L. Roukes, A. Y. Chtchelkanova, D. M. Treger, *Science*, 2001, **294**, 1488.
4. I. Zutic, J. Fabian, S. D. Sarma, *Rev. Mod. Phys*., 2004, **76**, 323.
5. M. N. Baibich, J. M. Broto, A. Fert, F. N. Van Dau, F. Petroff, P. Eitenne, G. Creuzet, A. Friederich and J. Chazelas, *Phys. Rev. Lett.*, 1988, **61**, 2472.
6. G. Binasch, P. Grünberg, F. Saurenbach and W. Zinn, *Phys. Rev. B,* 1989, **39**, 4828.
7. C. Chappert, A. Fert and F. N. Van Dau, *Nature Mater.*, 2007, **6**, 813.
8. A. Fert, *Rev. Mod. Phys*., 2008, **80**, 1517.
9. P. A. Gruenberg, *Rev. Mod. Phys*., 2008, **80**, 1531.
10. V. Dediu, M. Murgia, F. C. Matacotta, C. Taliani and S. Barbanera, *Solid State Communications*, 2002, **122**, 181.
11. Z. H. Xiong, D. Wu, Z. V. Vardeny, and J. Shi, *Nature*, 2004, **427**, 821.
12. V. A. Dediu, L. E. Hueso, I. Bergenti, and C. Taliani, *Nature Mater*., 2009, **8**, 707.
13. Z. Valy Vardeny, *Nature Mater*., 2009, **8**, 91.
14. F. J. Wang and Z. V. Vardeny, *Synth. Met*., 2010, **160**, 210.
15. E. Ehrenfreund and Z. V. Vardeny, *Phys. Chem. Chem. Phys.,* 2013, **15**, 7967.
16. F. J. Wang, Z. H. Xiong, D. Wu, J. Shi, and Z. V. Vardeny, *Synth. Met.,* 2005, **155**, 172.
17. P. Seneor, A. Bernand-Mantel and F. Petroff, *J. Phys.: Condens. Matter.,* 2007, **19**, 165222.
18. S. Bandyopadhyay, K. and M. Cahay, Introduction to Spintronics (CRC Press, 2008), 1st ed.
19. J.-H. Park, E. Vescovo, H.-J. Kim, C. Kwon,R. Ramesh, and T. Venkatesan, *Nature*, 1999, **392**, 794.
20. M. Bowen, M. Bibes, A. Barthelemy, J.-P. Contour, A. Anane, Y. Lemaıtre, and A. Fert. *Appl. Phys. Lett.*, 2003, **82**, 233.
21. Jung-Woo Yoo, Chia-Yi Chen, H.W. Jang, C.W. Bark, V. N. Prigodin,

C. B. Eom and A. J. Epstein, *Nature Mater.,* 2010, **9**, 639.
22. M. Urdampilleta, S. Klyatskaya, J-P. Cleuziou, M. Ruben, and W. Wernsdorfer, *Nature Mater.*, 2011, **10**, 502.
23. K. V. Raman, J. Chang, and J. S. Moodera, *Org. Electron*, 2011, **12**, 1275.
24. D. Waldron, P. Haney, B. Larade, A. MacDonald and H. Guo, *Phys. Rev. Lett.,* 2006, **96**,166804.
25. A. R. Rocha, V. M. Garcia-Suarez, S. W. Bailey, C. J. Lambert, J. Ferrer and S. Sanvito, *Nature Mater.,* 2005, **4**, 335.
26. C. Herrmann, G. C. Solomon and M. A. Ratner, *J. Am. Chem. Soc.,* 2010, **132**, 3682.
27. C. Herrmann, G. C. Solomon and M. A. Ratner, *J. Chem. Phys.,* 2011, **134**, 224306.
28. M. Smeu and G. A. Dilabio, *J. Phys. Chem. C,* 2010, **114**, 17874.
29. K. V. Raman, A. M. Kamerbeek, A. Mukherjee, N. Atodiresei, T. K. Sen, P. Lazic´, V. Caciuc, R. Michel, D. Stalke, S. K. Mandal, S. Bluegel, M. Munzenberg, and J. S. Moodera, *Nature*, 2013, **493**, 509.
30. E. Saitoh, M. Ueda, H. Miyajima, and G. Tatara, *Appl. Phys. Lett*., 2006, **88**, 182509.
31. Y. Kajiwara, K. Harii, S. Takahashi, J. Ohe, K. Uchida, M. Mizuguchi, H. Umezawa, H. Kawai, K. Ando, K. Takanashi, S. Maekawa, and E. Saitoh, *Nature,* 2010, **464**, 262.
32. K. Ando, S. Takahashi, J. Ieda, H. Kurebayashi, T. Trypiniotis, C. H.W. Barnes, S. Maekawa, and E. Saitoh, *Nature Mater.,* 2011, **10**, 655.
33. R. Godfrey and M. Johnson, *Phys. Rev. Lett.,* 2006, **96**, 136601
34. G. Schmidt, D. Ferrand, L. W. Molenkamp, A. T. Filip and B. J. van Wees, *Phys. Rev. B,* 2000, **62**, R4790
35. A. Fert and H. Jaffres, *Phys. Rev. B,* 2001, **64**, 184420
36. K. Ando, S. Watanabe, S. Mooser, E. Saitoh, and H. Sirringhaus, *Nature Mater.,* 2013, **12**, 622.
37. S. A. Crooker, E. S. Garlid, A. N. Chantis, D. L. Smith, K. S. M. Reddy, Q. O. Hu, T. Kondo, C. J. Palmstrøm, and P. A. Crowell, *Phys. Rev. B,* 2009, **80**, 041305R.
38. J. M. Kikkawa and D. D. Awschalom, *Nature,* 1999, **397**, 139.
39. J. Wang, A. Chepelianskii, F. Gao and N. C. Greenham, *Nature Comms*. 2012, **3**, 1191.
40. K. Uchida, S. Takahashi, K. Harii, J. Ieda, W. Koshibae, K. Ando, S. Maekawa and E. Saitoh, *Nature,* 2008, **455**, 778.
41. A. Slachter, F. L. Bakker, J. P. Adam and B. J. van Wees, *Nature Phys.,* 2010, **6**, 879.
42. J. Flipse, F. L. Bakker, F. K. Dejene and B. J. van Wees, *Nature Nanotech.,* 2012, **7**, 166.
43. M. Walter, J. Walowski, V. Zbarsky, M. Münzenberg, M. Schäfers, D. Ebke, G. Reiss, A. Thomas, P. Peretzki, M. Seibt, J. S. Moodera, M. Czerner, M. Bachmann and C. Heiliger, *Nature Mater.,* 2011, **10**,742.
44. G. E. W. Bauer, E. Sitoh and B. J. van Wees, *Nature Mater.,* 2012, **11**, 391.
45. F. L. Bakker, J. Flipse, A. Slachter, D. Wagenaar and B. J. van Wees, *Phys. Rev. Lett.,* 2012, **108**, 167602.
46. Y. Fukuma, L. Wang, H. Idzuchi, S. Takahashi, S. Maekawa and Y. C. Otani, *Nature Mater.,* 2011. **10**, 527.
47. A. Riminucci, M. Prezioso, C. Pernechele, P. Graziosi, I. Bergenti, R. Cecchini, M. Calbucci, M. Solzi, and V. Alek Dediu. *Appl. Phys. Lett.,* 2013, **102**, 092407.
48. X. Lou, C. Adelmann, S. A. Crooker, E. S. Garlid, J. Zhang, K. S. Madhukar Reddy, S. D. Flexner, C. J. Palmstrøm and P. A. Crowell. *Nature Phys.,* 2007, **3**, 197.
49. A. J. Drew, J. Hoppler, L. Schulz, F. L. Pratt, P. Desai, P. Shakya, T. Kreouzis, W. P. Gillin, A. Suter, N. A. Morley, V. K. Malik, A. Dubroka, K. W. Kim, H. Bouyanfif, F. Bourqui, C. Bernhard, R. Scheuermann, G. J. Nieuwenhuys, T. Prokscha and E. Morenzoni, *Nature Mater.,* 2009, **8**, 109.
50. M. Cinchetti, K. Heimer, J.-P. Wustenberg, O. Andreyev, M. Bauer, S. Lach, C. Ziegler, Y. Gao and M. Aeschlimann, *Nature Mater.,* 2009, **8**, 115.
51. Y. K. Kato, R. C. Myers, A. C. Gossard, and D. D. Awschalom, *Science,* 2004, **306**, 1910.
52. Yan Li, Y. Chye, Y. F. Chiang, K. Pi,W. H. Wang, J. M. Stephens, S. Mack, D. D. Awschalom, and R. K. Kawakami, *Phys. Rev. Lett.,* 2008, **100**, 237205.
53. Y. Li, W. Han, A. G. Swartz, K. Pi, J. J. I. Wong, S. Mack, D. D. Awschalom, and R. K. Kawakami, *Phys. Rev. Lett.,* 2010, **105**, 167203.
54. S. S. P. Parkin, C. Kaiser, A. Panchula, P. M. Rice, B. Hughes, M. Samant, and S.–H. Yang, *Nature Mater.,* 2004, **3**, 862.
55. S. S. P. Parkin, X. Jiang, C. Kaiser, A. Panchula, K. Roche, and M. Samant, *Proc. IEEE,* 2003, **91**, 661.
56. J. R. Petta, S. K. Slater and D. C. Ralph, *Phys. Rev. Lett.,* 2004, **93**,136601.
57. F. J. Wang, C. G. Yang, Z. V. Vardeny and X. G. Li, *Phys. Rev. B,* 2007, **75**, 245324.
58. W. Xu, G. J. Szulczewski, P. LeClair, I. Navarrete, R. Schad, G. Miao, H. Guo, and A. Gupta, *Appl. Phys. Lett*., 2007, **90**, 072506.
59. H. Vinzelberg, J. Schumann, D. Elefant, R. B. Gangineni, J. Thomas, and B. Büchner, *J. Appl. Phys.,* 2008, **103**, 093720.
60. J. S. Jiang, J. E. Pearson, and S. D. Bader, *Phys. Rev. B,* 2008, **77**, 035303.
61. J. H. Shim, K.V. Raman, Y. J. Park, T. S. Santos, G. X. Miao, B. Satpati, and J. S. Moodera, *Phys. Rev. Lett.*, 2008, 100, 226603.
62. Jung-Woo Yoo, H. W. Jang, V.N. Prigodin, C. Kao, C.B. Eom, and A.J. Epsteina, *Synth. Metal.* 2010, **160**, 216.
63. Jung-Woo Yoo, H. W. Jang, V. N. Prigodin, C. Kao, C. B. Eom, and A. J. Epstein, *Phys. Rev. B,* 2009, **80**, 205207.
64. J. J. H. M. Schoonus, P. G. E. Lumens, W. Wagemans, J. T. Kohlhepp, P. A. Bobbert, H. J. M. Swagten, and B. Koopmans. *Phys. Rev. Lett.,* 2009, **103**, 146601.
65. R. Lin, F. Wang, J. Rybicki, M. Wohlgenannt, and K. A. Hutchinson, *Phys. Rev. B*, 2010, **81**, 195214.
66. N. J. Harmon and M. E. Flatte, *Phys. Rev. Lett.,* 2012, **108**, 186602.
67. T. Lan Anh Tran, T. Quyen Le, Johnny G. M. Sanderink, Wilfred G. van der Wiel, and Michel P. de Jong. *Adv. Funct. Mater.,* 2012, **22**, 1180.
68. Sanvito, S. *Nature Phys.*, 2010, **6**, 562.
69. T. Ikegami, I. Kawayama, M. Tonouchi, S. Nakao, Y. Yamashita, and H. Tada, *Appl. Phys. Lett.,* 2008, **92**, 153304.
70. A. Ozbay, E. R. Nowak, Z. G. Yu, W. Chu, Yijian Shi, S. Krishnamurthy, Z. Tang, and N. Newman, *App. Phys. Lett.,* 2009, **95**, 232507.
71. K. S. Novoselov, A. K. Geim, S.V. Morozov, D. Jiang, Y. Zhang, S.V. Dubonos, I.V. Grigorieva, and A. A. Firsov, *Science*, 2004, **306**, 666.
72. K. S. Novoselov, A. K. Geim, S.V. Morozov, D. Jiang, M. I. Katsnelson, I.V. Grigorieva, S.V. Dubonos, and A. A. Firsov, *Nature*, 2005, **438**, 197.
73. D. Pesin and A. H. MacDonald. *Nature Mater.,* 2012, **11**, 409.
74. Y.-W. Son, M. L. Cohen, and S. G. Louie, *Nature*, 2006, **444**, 347.
75. W.Y. Kim and K. S. Kim, *Nature Nanotech*. 2008, **3**, 408.
76. N. Tombros, C. Jozsa, M. Popinciuc, H. T. Jonkman and B. J. van Wees, *Nature Phys*., 2007, **448**, 571-574.
77. M. Grobosch, K. Dorr, R. B. Gangineni, and M. Knupfer, *Appl. Phys. Lett.,* 2008, **92**, 23302.
78. M. V. Tiba, W. J. M. de Jonge, B. Koopmans, H. T. Jonkman, *J. Appl. Phys.,* 2006, **100**, 093707.
79. M. Popinciuc, H. T. Jonkman, and B. J. van Wees, *J. Appl. Phys.,* 2006, **100**, 093714.
80. W. Xu, J. Brauer, G. Szulczewski, M. S. Driver, and A. N. Caruso, *Appl. Phys. Lett.,* 2009, **94**, 233302.
81. Y. Q. Zhan, X. J. Liu, E. Carlegrim, F. H. Li, I. Bergenti, P. Graziosi, V. Dediu, and M. Fahlman, *Appl. Phys. Lett.,* 2009, **94**, 053301.
82. Y. Q. Zhan, M. P. de Jong, F. H. Li, V. Dediu, M. Fahlman, and W. R. Salaneck, *Phys. Rev. B,* 2008, **78**, 045208.
83. Y. Q. Zhan, I. Bergenti, L. E. Hueso, V. Dediu, M. P. de Jong, and Z. S. Li, *Phys. Rev. B,* 2007, **76**, 45406.
84. Y. -L. Chan, Y. –J. Hung, C. –H. Wang, Y. –C. Lin, C. -Y. Chiu, Y. –L. Lai, H. –T. Chang, C.-H. Lee, Y. -J. Hsu, and D.-H. Wei, *Phys. Rev. Lett.,* 2010, **104**, 177204.
85. J. S. Jiang, J. E. Pearson, and S. D. Bader, *Phys. Rev. Lett.,* 2011, **106**, 156807.
86. D. Wu, Z. H. Xiong, X. G. Li, Z.V. Vardeny, and Jing Shi, *Phys. Rev. Lett*. 2005, 95, 016802.
87. S. Majumdara, R. Laiho, P. Laukkanen, I. J. Väyrynen, H. S. Majumdar and R. Österbacka. *Appl. Phys. Lett.,* 2006, **89**, 122114.
88. S. Majumdar, H. Huhtinen, H. S. Majumdar, R. Laiho, and R. Österbacka1, *Appl. Phys. Lett.,* 2008, **92**, 153304.
89. F. Borgatti, I. Bergenti, F. Bona, V. Dediu, A. Fondacaro, S. Huotari G. Monaco, D. A. MacLaren, J. N. Chapman, and G. Panaccione.

Appl. Phys. Lett., 2010, **94**, 043306.
90. S. Majumdar, H. S Majumdar, R. Laiho and R. Österbacka, *New Journal of Physics,* 2009, **11**, 013022.
91. M. Grünewald, M. Wahler, F. Schumann, M. Michelfeit1, C. Gould1, R. Schmidt, F. Würthner, G. Schmidt, and L. W. Molenkamp, *Phys. Rev. B,* 2011, **84**, 125208.
92. G. Slis, S. F. Alvarado, M Tschudy, T. Brunschwiler and R. Allenspach, *Phys. Rev. B*, 2004, **70**, 085203.
93. Y. Liu, T. Lee, H. E. Katz, and D. H. Reich, *J. Appl. Phys*., 2009, **105**, 07C708.
94. Y. Liu, S. M. Watson, T. Lee, J. M. Gorham, H. E. Katz, J. A. Borchers, H. D. Fairbrother, and D. H. Reich, *Phys. Rev. B*, 2009, **79**, 075312.
95. T. Hosokai, H. Machida, A. Gerlach, S. Kera, F. Schreiber, and N. Ueno, *Phys. Rev. B,* 2011, **83**, 195310.
96. K. V. Raman, S. M. Watson, J. H. Shim, J. A. Borchers, J. Chang, and J. S. Moodera. *Phys. Rev. B,* 2009, **80**, 195212.
97. F. Li, P. Graziosi, Q. Tang, Y. Zhan, X. Liu, V. Dediu, and M. Fahlman, *Phys. Rev. B,* 2010, **81**, 205415.
98. T. Valet and A. Fert, *Phys. Rev. B,* 1993, **48**, 7099.
99. I. Lange, J. C. Blakesley, J. Frisch, A. Vollmer, N. Koch, and D. Neher, *Phys. Rev. Lett*., 2011, **106**, 216402.
100. P. A. Bobbert, W. Wagemans, F. W. A. van Oost, B. Koopmans, and M. Wohlgenannt. *Phys. Rev. Lett.,* 2009, **102**, 156604.
101. K. -S. Li, Y.-M. Chang, S. Agilan, J.-Y. Hong, J.-C. Tai, W.-C. Chiang, K. Fukutani, P. A. Dowben, and M. -T. Lin, *Phys. Rev. B,* 2011, **83**, 172404.
102. G. Szulczewski, S. Sanvito and J. M. D. Coey, *Nature Mater.,* 2009, **8**, 693.
103. P. A. Bobbert, W. Wagemans, F. W. A. Van Oost, B. Koopmans and M. Wohlgenannt, *Phys. Rev. Lett.,* 2009, **102**,156604.
104. X.-G. Zhang and S. T. Pantelides, *Phys. Rev. Lett.,* 2012, **108**, 266602.
105. W. Brütting, C. Adachi and R. J. Holmes, Physics of Organic Semiconductor (Wiley-VCH, Weinheim, 2012) 2nd ed.
106. P. Mark and W. Helfrich, *J. Appl. Phys*., 1962, **33**, 205-215.
107. M. Pope and C. E. Swenberg, Electronic Process in Organic Crystals and Polymers (Oxford University Press, Oxford, 1999), 2nd ed
108. P. W. M. Blom, M. J. M. de Jong, and J. J. M. Vleggaar, *Appl. Phys. Lett*., 1996, **68**, 3308-3310.
109. V. I. Arkhipov, E. V. Emelianova, Y. H. Tak, and H. Bässler, *J. Appl. Phys*., 1998, **84**, 848-856.
110. C. Boehme and J. M. Lupton, *Nature Nanotech.,* 2013, **8**, 612.
111. S. Pramanik, C.-G. Stefanita, S. Patibandla, S. Bandyopadhyay, K. Garre, N. Harth and M. Cahay, *Nature Nanotech.,* 2007, **2**, 216.
112. D. Sun, L. Yin, C. Sun, H. Guo, Z. Gai, X.-G. Zhang, T. Z. Ward, Z. H. Cheng, and J. Shen, *Phys. Rev. Lett.,* 2010, **104**, 236602.
113. V. Dediu, L. E. Hueso, I. Bergenti, A. Riminucci, F. Borgatti, P. Graziosi, C. Newby, F. Casoli, M. P. De Jong, C. Taliani, and Y. Zhan, *Phys. Rev. B*, 2008, **78**, 115203.
114. C. Barraud, P. Seneor, R. Mattana, S. Fusil, K. Bouzehouane, C. Deranlot, P. Graziosi, L. Hueso, I. Bergenti, V. Dediu, F. Petroff and A. Fert, *Nature Phys*., 2010, **6**, 615.
115. S. Steil, N. Großmann, M. Laux, A. Ruffing, D. Steil, M. Wiesenmayer, S. Mathias, O. L. A. Monti, Mi. Cinchetti, and M. Aeschlimann, *Nature Phys.,* 2013, **9**, 242.
116. M. Julliere, *Phys. Letters A*, 1975, **54**, 225-226.
117. T. D. Nguyen, G. Hukic-Markosian, F. Wang, L. Wojcik, X.-G. Li, E. Ehrenfreund and Z. Valy Vardeny, *Nature Mater*, 2010, **9**, 345.
118. T. D. Nguyen, F. Wang, X.-G. Li, E. Ehrenfreund and Z. V. Vardeny, *Phys Rev B*, 2013, **87**, 075205.
119. S. Duffe, N. Groenhagen, L. Patryarcha, B. Sieben, C. Yin, B. von Issendorff, M. Moseler, and H. Hoevel, *Nature Nano*. 2010, **5**, 335.
120. D. Huertas-Hernando, F. Guinea and A. Brataas, *Phys. Rev. B*, 2006, **74**, 155426.
121. W. H. Butler, X.-G. Zhang, T. C. Schulthess, and J. M. MacLaren, *Phys. Rev. B,* 2001, **63**, 054416.
122. S. Ikeda, J. Hayakawa, Y. Ashizawa, Y. M. Lee, K. Miura, H. Hasegawa, M. Tsunoda, F. Matsukura, and H. Ohno, *Appl. Phys. Lett*., 2008, **93**, 082508.
123. N. A. Morley, A. Rao, D. Dhandapani, M. R. J. Gibbs, M. Grell and T. Richardson, *J. Appl. Phys.*, 2008, **103**, 07F306.
124. M. Grünewald, J. Kleinlein, F. Syrowatka, F. Würthner, L.W. Molenkamp, and G. Schmidt, arXiv:1304.2911
125. B. B. Chen, Y. Zhou, S. Wang, Y. J. Shi, H. F. Ding, and D. Wu, *Appl. Phys. Lett*., 2013, **103**, 072402.
126. T. S. Santos, J. S. Lee, P. Migdal, I. C. Lekshmi, B. Satpati, and J. S. Moodera, *Phys. Rev. Lett.,* 2007, **98**, 016601.
127. G. Szulczewski, H. Tokuc, K. Oguz, and J. M. D. Coey, *Appl. Phys. Lett*., 2009, **95**, 202506.
128. X. Zhang, S. Mizukami, T. Kubota, Q. Ma, M. Oogane, H. Naganuma, Y. Ando and T. Miyazaki, *Nature Comms*. 2012, **4,** 1392.
129. Ö. Mermer, G. Veeraraghavan, T. L. Francis, Y. Sheng, D. T. Nguyen, M. Wohlgenannt, A. Köhler, M. K. Al-Suti, and M. S. Khan, *Phys. Rev. B*, 2005, **72**, 205202.
130. T. D. Nguyen, Y. Sheng, J. Rybicki, and M. Wohlgenannt, *Phys. Rev. B*, 2008, **77**, 235209.
131. S. P. Kersten, S. C. J. Meskers, and P. A. Bobbert, *Phys. Rev. B*, 2013, **86**, 045210.
132. R. N. Mahato, H. Lülf, M. H. Siekman, S. P. Kersten, P. A. Bobbert, M. P. de Jong, L. De Cola, W. G. van der Wiel, *Science,* 2013, **241**, 257.
133. J. Rybicki, R. Lin, F. Wang, M. Wohlgenannt, C. He, T. Sanders, and Y. Suzuki, *Phys. Rev. Lett.*, 2012, **109**, 076603.
134. F. Wang, F. Macia, M. Wohlgenannt, A. D. Kent, and M. E. Flatte, *Phys. Rev. X,* 2012, **2**, 021013.
135. F. Macia, F. Wang, N. J. Harmon, M. Wohlgenannt, A. D. Kent, and M. E. Flatte, *Appl. Phys. Lett.,* 2013, **102**, 042408.
136. N. J. Harmon, F. Macia, F. Wang, M. Wohlgenannt, A. D. Kent, and M. E. Flatte, *Phys. Rev. B,* 2013, **87**, 121203R.
137. L. E. Hueso, I. Bergenti, A. Riminucci, Y. Zhan, and V. Dediu, *Adv. Mater.*, 2007, **19**, 2639.
138. M. Prezioso, A. Riminucci , I. Bergenti , P. Graziosi , D. Brune, and V. A. Dediu, *Adv. Mater.,* 2011, **23**, 1371.
139. M. Prezioso, A. Riminucci, P. Graziosi, I. Bergenti, R. Rakshit, R. Cecchini, A. Vianelli, F. Borgatti, N. Haag, M. Willis, A. J. Drew, W. P. Gillin, and V. A. Dediu. *Adv. Mater.,* 2013, **25**, 534.
140. L. Schulz, L. Nuccio, M.Willis, P. Desai, P. Shakya, T. Kreouzis, V. K. Malik, C. Bernhard, F. L. Pratt, N. A. Morley, A. Suter, G. J. Nieuwenhuys, T. Prokscha, E. Morenzoni, W. P. Gillin and A. J. Drew, *Nature Mater.,* 2011, **10**, 39.
141. H. –J. Jang, K. P. Pernstich, D. J. Gundlach, O. D. Jurchescu, and C. A. Richter, *Appl. Phys. Lett.,* 2012, **101**, 102412.
142. D. Pantel, S. Goetze, D. Hesse, and M. Alexe, *Nature Mater.,* 2012, **11**, 289.
143. D. Sun, X. Xu, L. Jiang, H. Guo, H. N. Lee, P. C. Snijders, T. Z. Ward, Z. Gai, X.-G. Zhang, and J. Shen, *arXiv:1304.2446.*
144. B. F. Ding, Y. Q. Zhan, Z. Y. Sun, X. M. Ding, X. Y. Hou, Y. Z. Wu, I. Bergenti, and V. Dediu, *Appl. Phys. Lett.,* 2008, **93**. 183307.
145. T. D. Nguyen, E. Ehrenfreund, and Z. V. Vardeny, *Science,* 2012, **337**, 204.
146. R. H. Friend, R. W. Gymer, A. B. Holmes, J. H. Burroughes, R. N. Marks, C. Taliani, D. D. C. Bradley, D. A. Dos Santos, J. L. Brédas, M. Lögdlund and W. R. Salaneck, *Nature,* 1999, **397**, 121.
147. S. R. Forrest, *Nature*, 2004, **428**, 911.
148. K. M. Alam and S. Pramanik, *Phys. Rev. B,* 2011. **83**, 245206.
149. D. Sun, T. P. Basel, B. R. Gautam, W. Han, X. Jiang, S. S. P. Parkin, and Z. Valy Vardeny, *Appl. Phys. Lett.,* 2013, **103**, 042411.

